Petroleum Science 21 (2024) 2130–2138

Contents lists available at ScienceDirect

Petroleum Science

journal homepage: www.keaipublishing.com/en/journals/petroleum-science

Original Paper

A molecular insight into coke formation process of vacuum residue in thermal cracking reaction

Ji-Guang Li*, Xin Guo, Huan-Di Hou

Heavy Oil Processing Department, Sinopec Research Institute of Petroleum Processing Co., Ltd, Beijing, 100083, China

ARTICLE INFO

Article history:
Received 5 April 2023
Received in revised form
25 September 2023
Accepted 29 January 2024
Available online 20 February 2024

Edited by Jia-Jia Fei and Min Li

Keywords:
Vacuum residue
Thermal cracking
Asphaltene
Coking induction period
Sulfur
Nitrogen

ABSTRACT

Understanding the coking behaviors has been considered to be really essential for developing better vacuum residue processing technologies. A battery of thermal cracking tests of typical vacuum residue at 410 °C with various reaction time were performed to evaluate the coke formation process. The total yields of ideal components including naphtha, atmospheric gas oil (AGO) and vacuum gas oil (VGO) of thermal cracking reactions increased from 10.89% to 40.81%, and the conversion ratios increased from 8.05% to 43.33% with increasing the reaction time from 10 to 70 min. The asphaltene content increased from 12.14% to a maximum of 22.39% and then decreased, and this maximum of asphaltene content occurred at the end of the coking induction period. The asphaltenes during the coking induction period, at the end and after coking induction period of those tested thermal cracking reactions were characterized to disclose the structure changing rules for coke formation process, and the coke formation pathways were discussed to reveal the coke formation process at molecular level.

1. Introduction

Nowadays, with the energy emergency, rising oil prices, the growth of motor fuel demand, and increasingly rigorous environmental laws and regulations, vacuum residue (VR) deep processing technologies are attracting more and more attention in global oil refining industry (Rana et al., 2007; Sahu et al., 2015; Gkillas et al., 2022). While, coking is always a main problem which can cause reduction of product yield, plugging or fouling for equipments and deactivation of catalyst (Gonçalves et al., 2007; Wang et al., 2018; Yang et al., 2022). The operating stability for vacuum residue processing technologies such as thermal cracking and hydrotreating process could be greatly influenced for coke formation (Marques et al., 2011; Xu, 2018; Prajapati et al., 2021; Wang F. et al., 2021; Wang L.T. et al., 2021; Chesnokov et al., 2022), and the coking problems can greatly influence the economy and feasibility of vacuum residue processing technology. Thermal racking technology is still core technology for inferior raw material processing (Forero-Franco et al., 2023; Zhong et al., 2023). Coking behaviors of VR's thermal cracking process provide a good reference for the other vacuum residue's processing technologies, and understanding the coking behaviors of vacuum residue has been considered to be really essential for developing better long-term running VR processing technologies (Wang et al., 2020).

Wiehe proposed the coke formation mechanism through the combination of chemical reactions of VR's thermal cracking process, and further described that it will occur phase separation when the concentration of asphaltene exceeds a critical limit after coking induction period and a new mesophase is produced and coke (toluene insoluble) formation follows rapidly (Wiehe, 1993; Wiehe and Liang, 1996). While, three decades have passed, the coke formation process is stilled puzzled for the asphaltene structure changing rules during this process. It is widely recognized that asphaltene molecules are the coke precursors and the major contributors to coke formation for thermal cracking and hydrocracking process (Yasar et al., 2000; Guo et al., 2008; Wang F. et al., 2021; Wang L.T. et al., 2021; Yang et al., 2022). Asphaltenes that are defined by solubility are the crude oil/vacuum residue fractions insoluble in *n*-heptane but soluble in toluene (Buenrostro-Gonzalez et al., 2001; Chacon-Patino et al., 2015), tend to combine with heteroatom-containing heterocycles (Mandal et al., 2012; Zhao et al., 2013; Wang F. et al., 2021; Wang L.T. et al., 2021). It is found that stable aggregates could be formed for asphaltenes, and a supramolecular assembly behavior of asphaltene molecules

* Corresponding author.
E-mail address: lijiguang.ripp@sinopec.com (J.-G. Li).

https://doi.org/10.1016/j.petsci.2024.01.023

coupled with cooperative binding, and π-stacking interactions play an important role in forming stable asphaltene aggregates (Mullins, 2010; Gray et al., 2011; Pomerantz et al., 2015). Asphaltene aggregation behaviors restrict comprehensive structural characterization of those asphaltene molecules (Cosultchi et al., 2002; Hortal et al., 2007; Dechaine and Gray, 2010; Chacon-Patino et al., 2015).

In this work, thermal cracking tests of vacuum residue at various reaction time were performed to evaluate the coke formation process. Both thermal cracking process and slurry phase hydrocracking (SHC) process are considered to follow free radical reactions (Du et al., 2015; Kaminski and Husein, 2019; Wang F. et al., 2021; Wang L.T. et al., 2021), and special SHC tests were conducted to examine the shift of coking induction period for thermal cracking reaction. The asphaltenes of thermal cracking reactions were characterized by fourier transform ion cyclotron resonance mass spectroscopy (FT-ICR MS) to disclose the coke formation process at molecular level.

2. Experimental procedure

2.1. Materials

All the toluene and *n*-heptane (abbreviation for heptane) used for asphaltene and toluene insoluble separation were claimed more than 99% purity, supported by Sinopharm Chemical Reagent Co., Ltd. The vacuum residue tested in this work, from Middle East, is a typical inferior VR with C7-asphaltene content of 10.1% (ASTM D6560 method), the residual carbon content of 24.35% (GB/T17144 method), hydrogen content of 9.86% (SH/T0656 method) and about 96.5% > 524 °C fractions (obtained by ASTMD7169 method listed in S-1 of supporting information).

2.2. Experimental route and methods

As illustrated in Scheme 1, the VR were heated in an oven at 160 °C for 2 h to make sure the VR were fluid with low viscosity. All the reactions were carried out in a 1.8 L batch-type autoclave reactor. For thermal cracking reactions, 250 g VR were added in the reactor. The air in the reactor was displaced with nitrogen for 5 times, and then the reactor was filled with 0.2 MPa nitrogen. For SHC reaction, 250 g VR and 1 g catalyst (molybdenum octoate catalyst with Mo content of 15.0%) were added in the reactor. The air in the reactor was displaced with nitrogen and hydrogen for 3 times respectively, and then the reactor was filled with 8 MPa hydrogen (Li J. et al., 2022; Li J.G. et al., 2022). It would cost about 50 min from room temperature to 410 °C and the residence time was started at the point of reaching 410 °C. The residence time ranged from 10 to 70 min, and rotation speed was running at 500 rpm. After reactions, the operator should release the gas smoothly and collect the liquid products. As shown in Scheme 1, the asphaltene content, asphaltene samples for analysis and toluene insoluble (TI) content of the reaction products were obtained by ASTM D6560 standard. A Bruker SolariX XR-15T fourier transform ion cyclotron resonance mass spectroscopy (FT-ICR MS) with $APPI^+$ source was utilized to analyze the asphaltene structures.

3. Results and discussion

3.1. Coking induction period determined for thermal cracking reactions

For getting products with ordered distribution, thermal cracking reactions of VR at 410 °C with various reaction time were performed according to plenty of exploration tests. The liquid products of thermal cracking reactions were shown in Fig. 1, and the product of 70 min reaction appeared small sand-like solid in the liquid surface.

Thermal cracking reactions with various reaction time were carried out and the reaction results were indicated in Table 1. The conversion ratios of those thermal reactions were determined by Eq. (1), where $m_{>524\ °C\ fractions}$ represented the mass fractions of > 524 °C distillates obtained by simulated distillation of ASTM D7169 method.

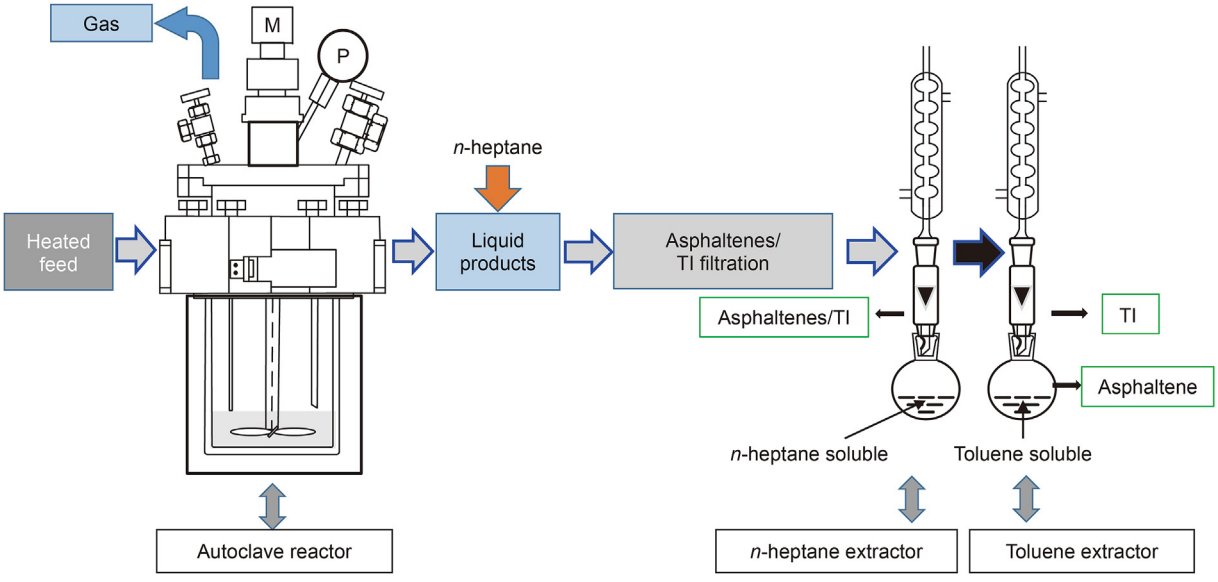

Scheme 1. The main experimental route and methods.

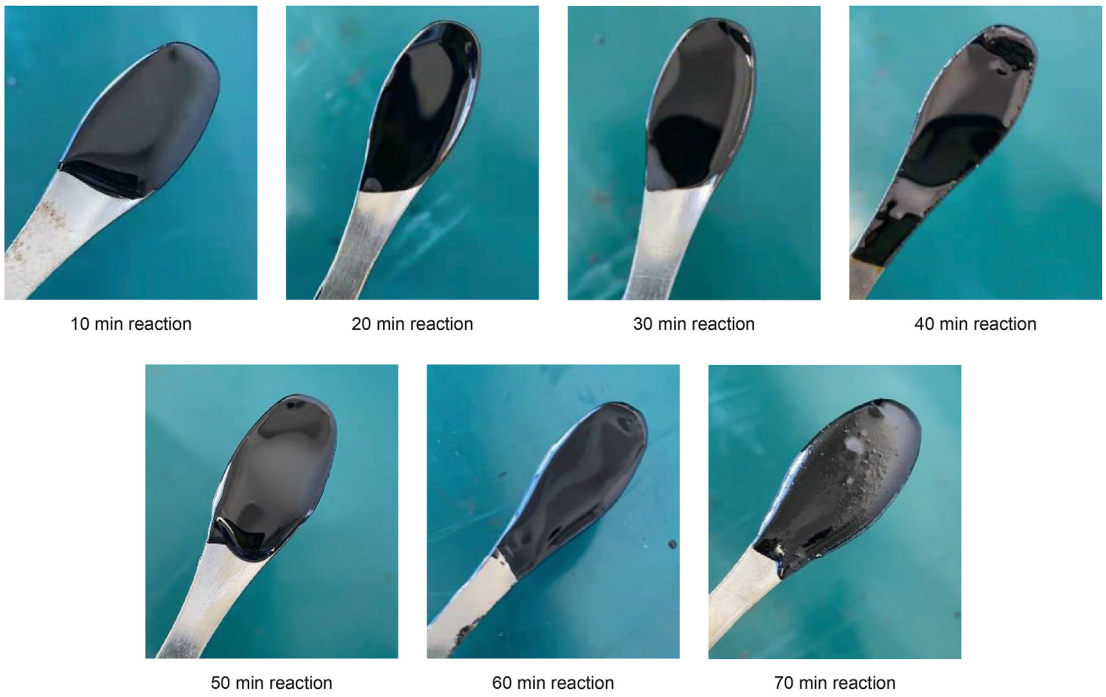

Fig. 1. The thermal cracking products from the autoclave.

Table 1
Material balance of 10–70 min reactions.

Reaction time, min	10	20	30	40	50	60	70
Mass distribution, wt%							
Gas	1.02	2.35	2.85	3.51	4.18	4.54	4.90
Naphtha (IBP–180 °C)	2.47	1.08	3.40	3.68	5.05	5.70	6.18
AGO (180–350 °C)	3.42	4.56	8.07	14.27	14.72	15.04	16.05
VGO (350–524 °C)	5.00	10.06	13.06	14.09	19.60	20.02	18.58
Tailing (>524 °C)	88.09	81.95	72.62	64.45	56.45	54.70	54.29
Total, %	100.00	100.00	100.00	100.00	100.00	100.00	100.00
Conversion ratio, %	8.05	14.45	24.20	32.73	41.08	42.90	43.33

$$\text{Conversion ratio} = \frac{m_{>524\,^\circ C\text{ fractions of the feed}} - m_{>524\,^\circ C\text{ fractions of the product}}}{m_{>524\,^\circ C\text{ fractions of the feed}}} \quad (1)$$

As prolonging the reaction time, gas, naphtha and AGO yields kept a steady increase and the tailing yields kept decrease. The total yields of ideal components (naphtha, AGO and VGO) of thermal cracking reactions increased from 10.89% to 40.81%, and the conversion ratios increased from 8.05% to 43.33% with increasing the reaction time from 10 to 70 min. It could conclude that 40 min reaction appeared to be the most vital node for the yields of TI and asphaltenes in Fig. 2, and the coking induction time could be about 40 min. As seen in Table 1, the AGO yield seemed to change fast during coking induction time but a bit slowly after coking induction time.

Fig. 2 showed the yields of TI and asphaltenes vs. reaction time. It was observed a coking induction period of 40 min for thermal racking reaction. With prolonging the reaction time, the coke yield increased slightly during coking induction period, and increased significantly after coking induction period. The coke formation derived of asphaltenes condensation in thermal cracking process could be regarded to be the first order reaction, and higher asphaltene content could accelerate coke formation (Yasar et al., 2001; Kaminski and Husein, 2019). The asphaltene content increased from 12.14% to a maximum of 22.39% and then decreased, and this maximum of asphaltene content occurred at the end of the coking induction period for both thermal cracking reaction and SHC reaction (Wiehe, 1993; Yang et al., 2022). Both thermal cracking reaction and slurry phase hydrocracking reaction follow free radical reaction (Wiehe, 1993; Du et al., 2015; Kaminski and Husein, 2019; Wang F. et al., 2021; Wang L.T. et al., 2021; Yang et al., 2022), and for comparison, a series of SHC reactions were performed with reaction temperature of 410 °C and reaction time from 10 to 70 min. As seen in Fig. 2, the asphaltene content could be greatly reduced and TI yields were also radically reduced for SHC process, and SHC process can greatly prolong the induction period.

Except for asphaltene content, asphaltene structures could also

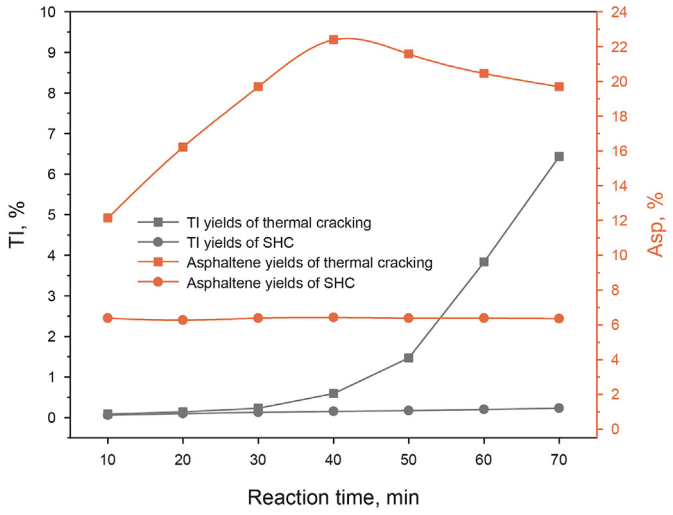

Fig. 2. The yields of TI and asphaltenes vs. reaction time.

play important role in coke formation process. For further understanding the coke formation process, the asphaltene structures for thermal cracking process were analyzed by FT-ICR MS.

3.2. Asphaltene changing rules before and after coking induction period

3.2.1. Sulfur class of asphaltene changing rules

FT-ICR MS has been proved effective to characterize asphaltene molecules (Rogel and Witt, 2017; Chacón-Patiño et al., 2020; Niles et al., 2020). For learning the structure changing rules of asphaltenes during and at the end and after coking induction period, FT-ICR MS was utilized to characterize the asphaltenes. As shown in Fig. 3, representative aromatic classes (listed in S-2 of supporting information) of asphaltenes for 10, 20, 30, 40, 50, 60, and 70 min reactions (short for Asp-10, Asp-20, Asp-30, Asp-40, Asp-50, Asp-60, and Asp-70 respectively) were examined, and S1 to S4 classes were the most abundant aromatic classes. Clearly, a remarkable decrease for the relative abundance of S2 to S4 classes of Asp-10 to Asp-30 respectively were observed, and correspondingly S1 class

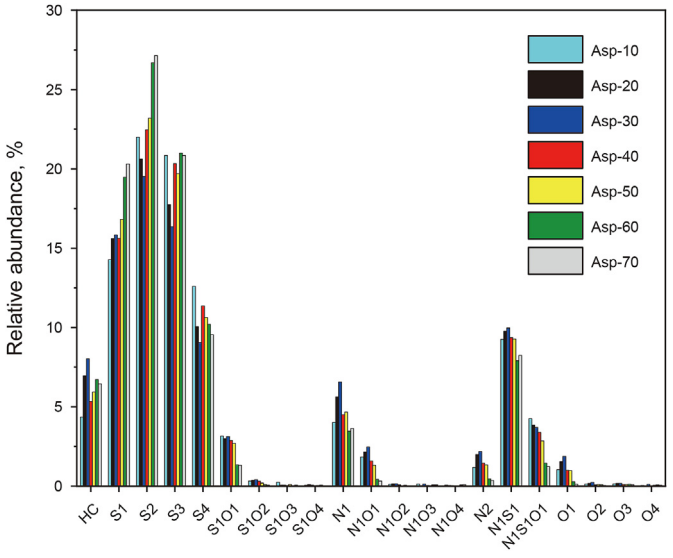

Fig. 3. The components of asphaltenes from Asp-10 to Asp-70 by FT-ICR MS.

were getting higher. S2 and S3 and S4 species showed much higher conversion ratios, which was agreed with that of thermal cracking and fixed-bed hydrocracking reactions (Zhang et al., 2020; Zhao et al., 2021; Jung et al., 2022; Li J. et al., 2022; Li J.G. et al., 2022). S1 class were difficult to convert , and S2 and S3 and S4 classes were classified into easily-converted aromatic sulfur compounds for smaller space hindered effect (Jung et al., 2022; Rogel and Witt, 2017; Zhang et al., 2020; Zhao et al., 2021). S1 class could also be newly generated from the conversion of S2, S3 and S4 class species, which could be the reason that correspondingly relative abundance of S1 species were getting higher and higher.

Double bond equivalent (DBE) versus carbon number (CN) distribution of S1 and S2 and S3 and S4 classes were shown in Figs. 4–7 respectively, and typical aromatic structure and the recommended formula for calculating DBE were listed in S-2 of supporting information. As seen in Figs. 4–7, the distributions of CN and DBE varied approximately from 23 to 68 and 15 to 41 respectively for S1 to S4 class compounds. As seen in Fig. 8, from Asp-10 to Asp-70, the values of Ave. CN of S1 to S4 classes decreased slightly. From Asp-30 to Asp-70, (Ave. DBE)/(Ave. CN) values representing the aromaticity of S1 and S2 and S3 and S4 class species got slightly higher with a little bit of fluctuations from Asp-10 to Asp-30, and the growth of (Ave. DBE)/(Ave. CN) values should be attributed to combined reactions of polycondensation and lateral chain break reactions (Li J. et al., 2022; Li J.G. et al., 2022; Smyshlyaeva et al., 2022).

As seen in Figs. 8 and 9, Ave. CN and sulfur content both got lower from Asp-10 to Asp-30, which could be the reason that relative abundance of S2 and S3 and S4 classes showed a remarkable decrease from Asp-10 to Asp-30 as illustrated in Fig. 2. As listed in Table 1, from 40 min reaction, the conversion ratio was more than 30%, and the dealkylation reaction began to accelerate. The remaining S2 and S3 and S4 classes were hard to convert from Asp-40 to Asp-70, which could be further proved by sulfur content changing rules shown in Fig. 9. The faster dealkylation speed could be a key reason for the increase of relative abundance of S-containing structures from 40 min reaction, and N-containing (N1, N1S1, N1O1 and N1S1O1) classes' significant decrease shown in Fig. 2 could be another reason for the increase of S-containing classes.

3.2.2. Nitrogen class of asphaltene changing rules

Asphaltene with higher polarity has a larger tendency to precipitate and form deposits (Wattana et al., 2005). N-containing classes (N1, N1S1, N1O1 and N1S1O1) are the most abundant polar compounds in asphaltenes. For further analyzing the relative abundance and structure changing rules of asphaltenes during, at the end and after coking induction period, CN and DBE distributions and their calculated parameters of N1 class were shown in Figs. 10–12 respectively.

As shown in Figs. 10 and 11, the distributions of CN and DBE varied approximately from 30 to 64 and from 18 to 40 respectively for N1 class species. As seen in Fig. 11, with increasing the reaction time, the quantity of structures with DBE $\geq$36 got higher and higher from Asp-10 to Asp-50, but got disappeared for A-60 and A-70. As seen in Fig. 12, (Ave. DBE)/(Ave. CN) of N1 species got slightly increase with increasing reaction time from Asp-30 and Asp-70.

Clearly, the relative abundance of N1 class had an increase from Asp-10 to Asp-30 but a decrease from Asp-40 to Asp-70 as shown in Fig. 2, which agreed with the changing rules for Ave. CN and nitrogen content as shown in Figs. 12 and 13 respectively. From Asp-40 to Asp-70, the asphaltenes formed more coke (TI), which would involve the decrease of N1 class and the reduction of nitrogen content for condensation reaction or phase separation as illustrated in Figs. 12 and 13.

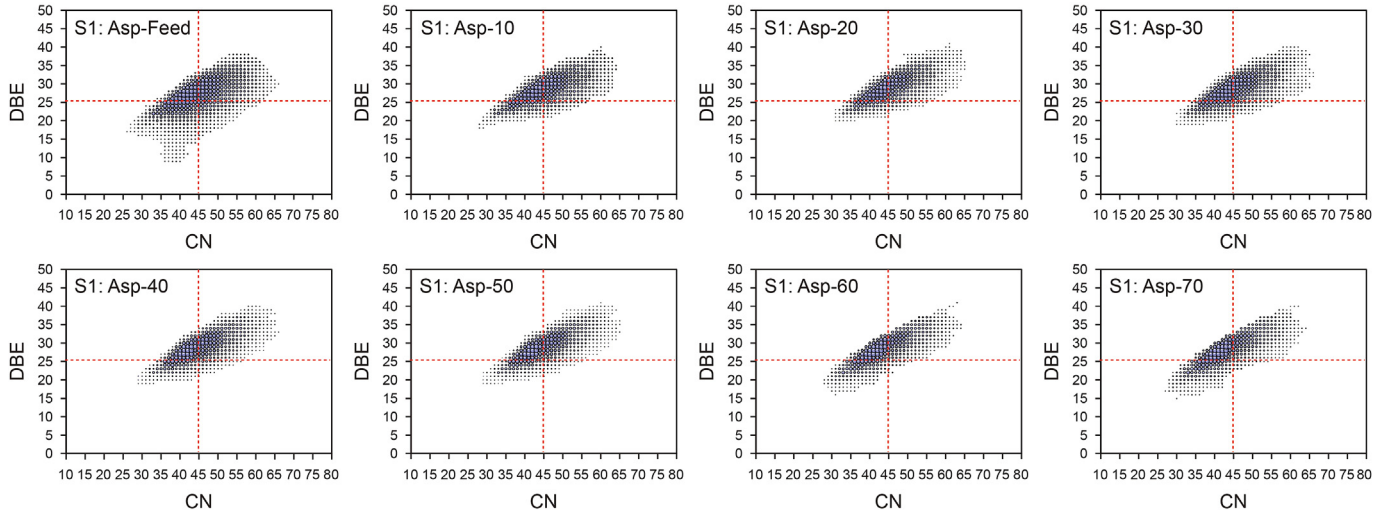

Fig. 4. DBE vs. CN distribution of S1 compounds.

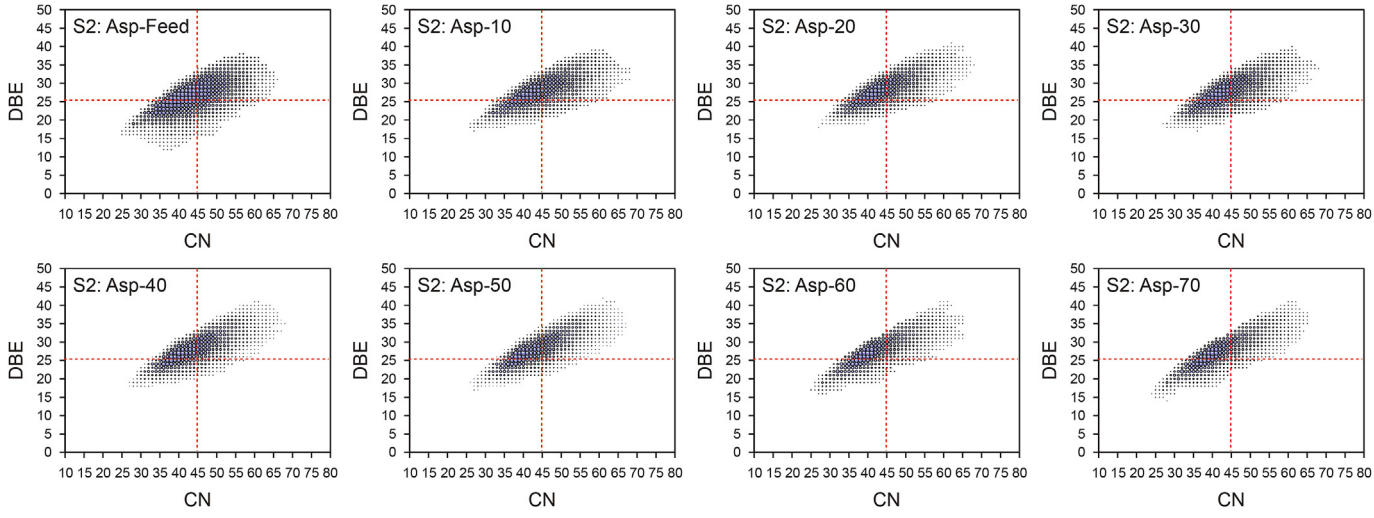

Fig. 5. DBE vs. CN distribution of S2 compounds.

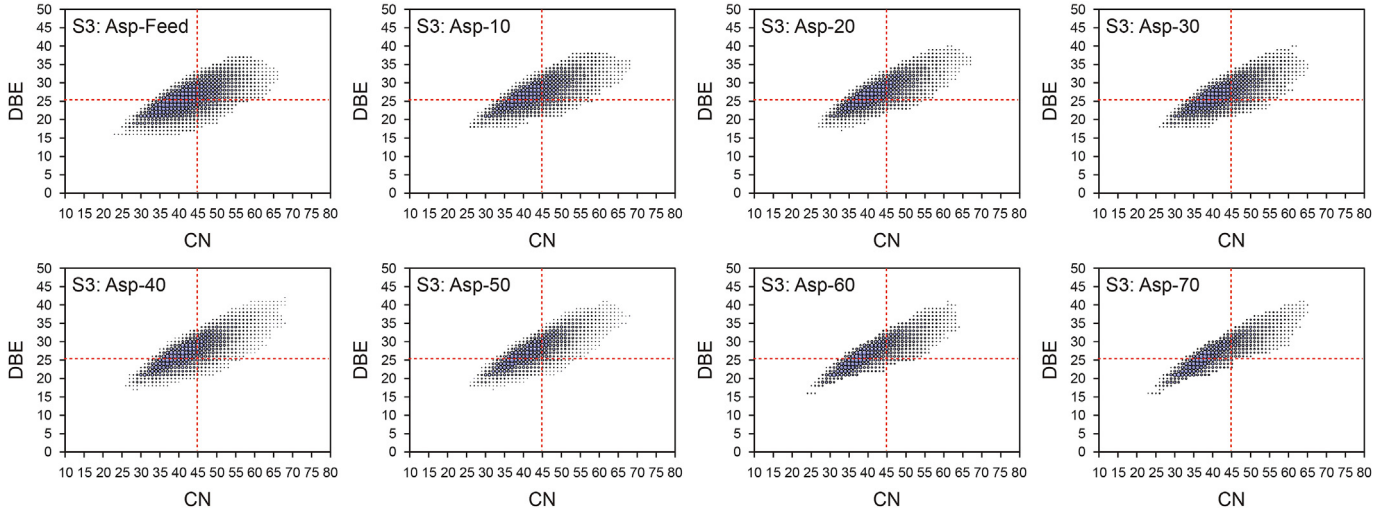

Fig. 6. DBE vs. CN distribution of S3 compounds.

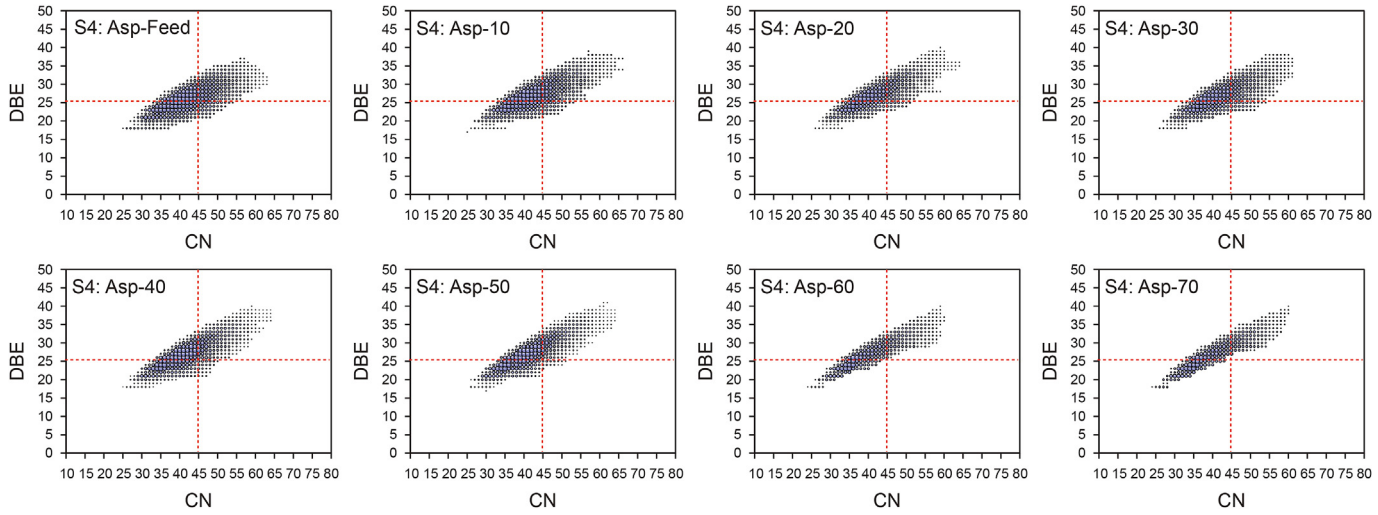

Fig. 7. DBE vs. CN distribution of S4 compounds.

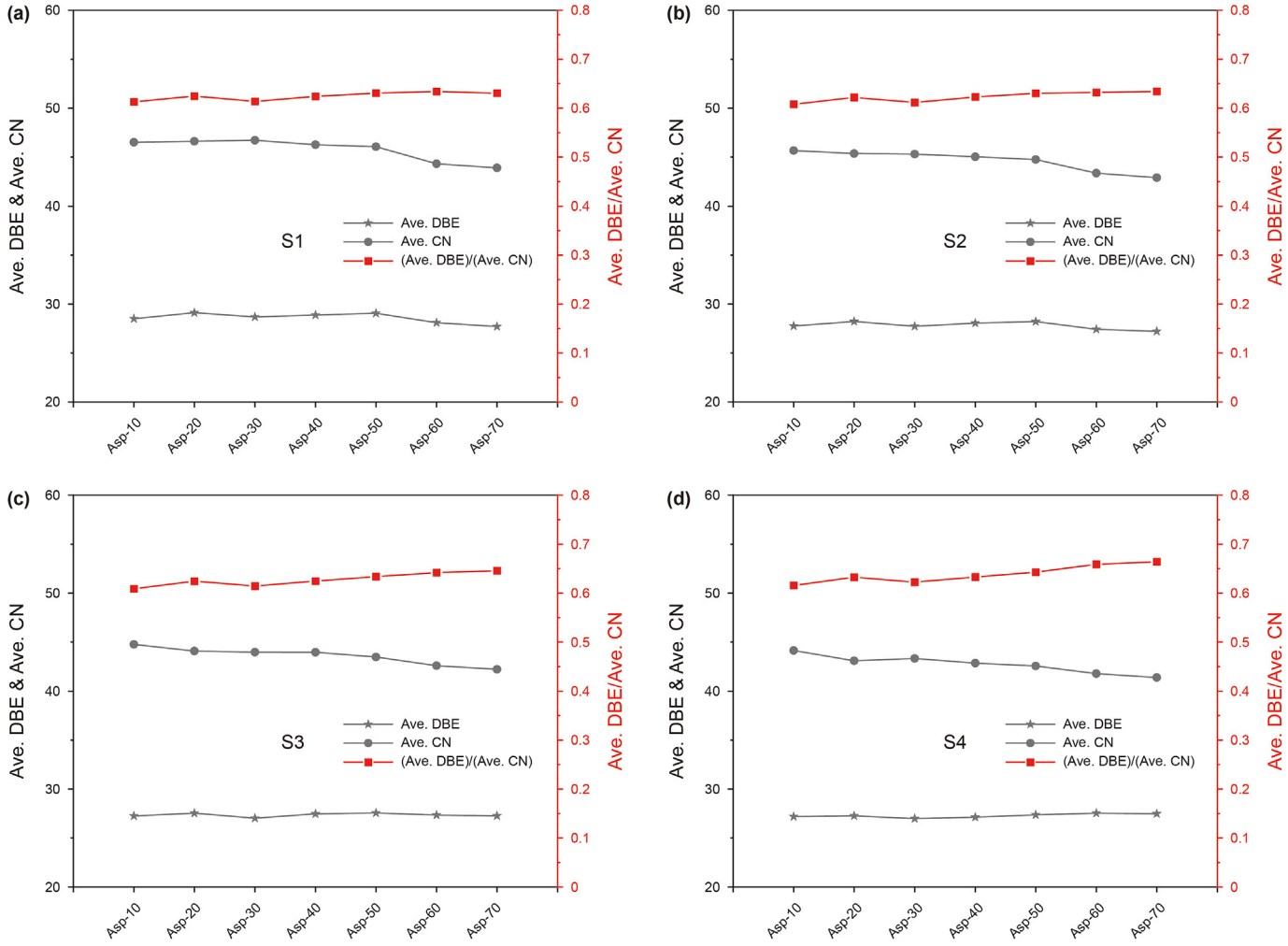

Fig. 8. Ave. DBE, Ave. CN and Ave. DBE/Ave. CN of S1, S2, S3 and S4 compounds respectively.

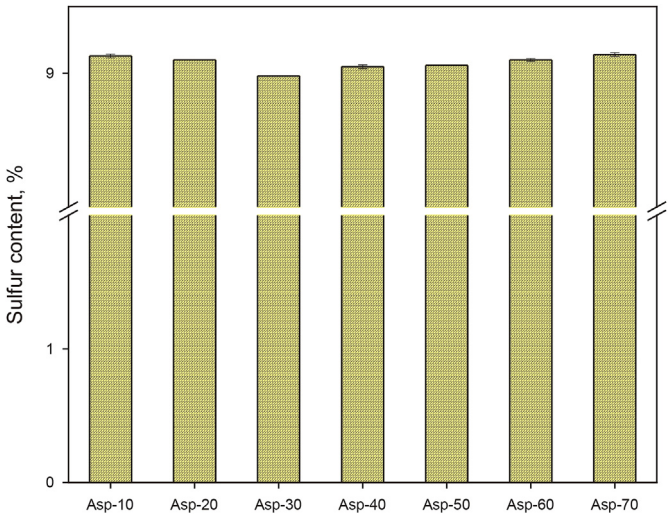

Fig. 9. Sulfur content with error bars (The method was listed in S-3 of supporting information) of asphaltenes from Asp-10 to Asp-70.

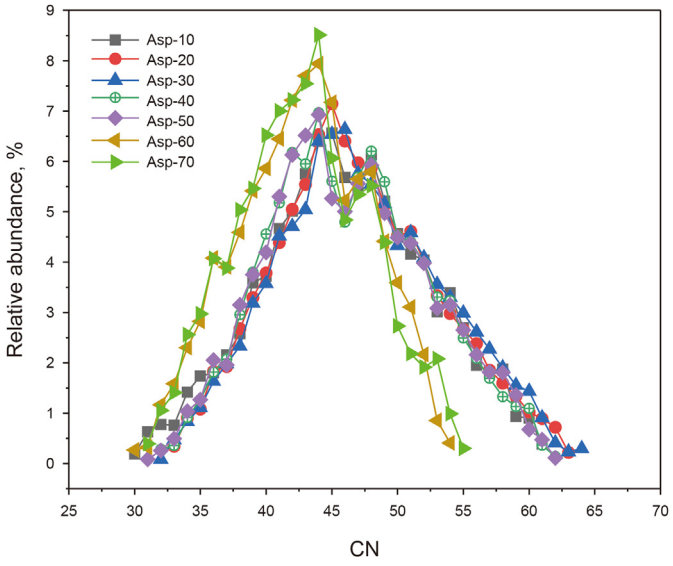

Fig. 10. CN distributions of N1 compounds.

3.3. Coke formation pathways during thermal cracking reaction

In Fig. 11, unlike S1 to S4 structures, there were no DBE>36 structures in N1 species for Asp-10 and Asp-60 and Asp-70, and the quantity of N1 structures with DBE≥36 got higher and higher from Asp-20 to Asp-50. The disappearance of N1 structures with DBE>36 of Asp-60 and Asp-70 should be attributed to those structures' condensation for coke formation or deposit from the liquids, and N1 structures with 36≤DBE≤40 could be taken as coke intermediates which could be changed to more condensed aromatic structures of coke or taken as true coke.

Combined with the analysis of Figs. 10 to 12, the coke formation process is a continuous process with 40 min reaction as the turning point for coke formation. The N1 structures with DBE = 36 were the most abundant among those DBE≥36 structures of N1 class for Asp-40 of 40 min reaction as illustrated in Fig. 11. CN distribution of N1 structures with DBE = 36 for Asp-40 were illustrated in Fig. 14, and the most abundance species were located at CN = 50. The

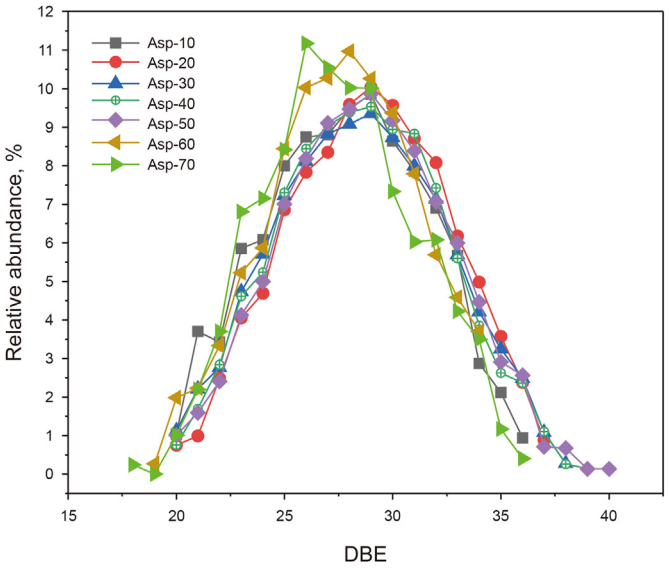

Fig. 11. DBE distributions of N1 compounds.

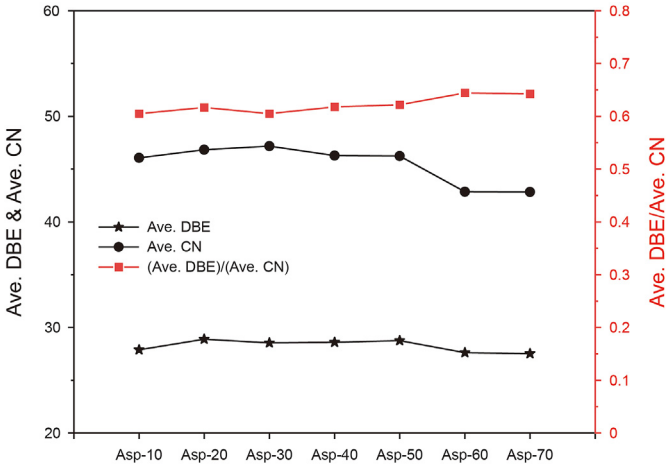

Fig. 12. Ave. DBE, Ave. CN and Ave. DBE/Ave. CN of N1 compounds.

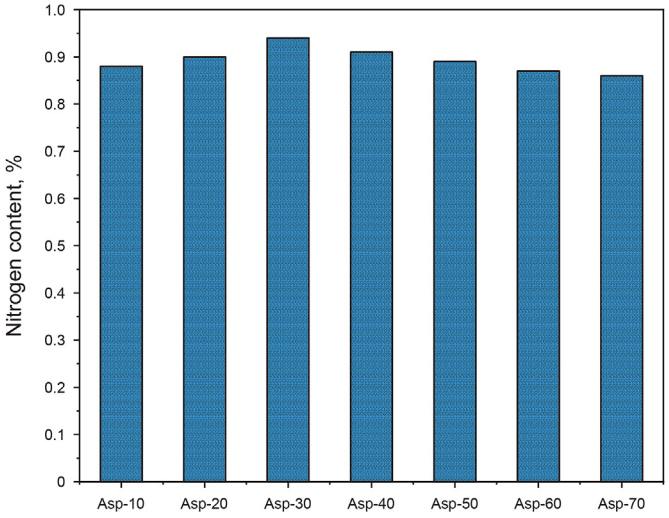

Fig. 13. Nitrogen content (obtained by SH/T 0656 method) of asphaltenes from Asp-10 to Asp-70.

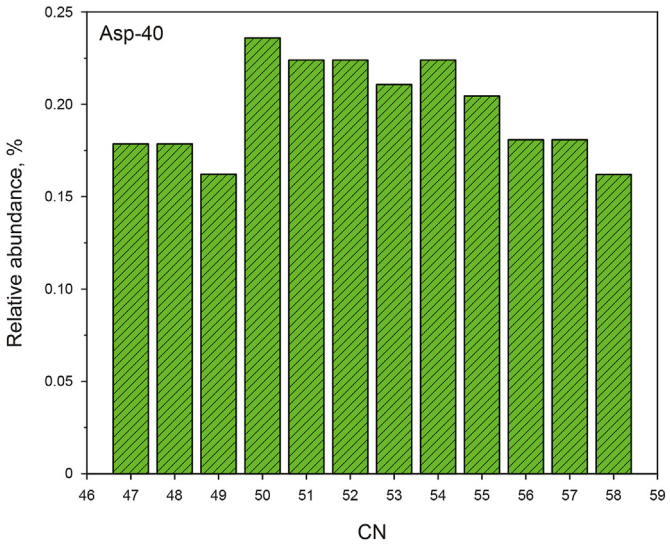

Fig. 14. CN distribution of N1 structures with DBE = 36 for Asp-40.

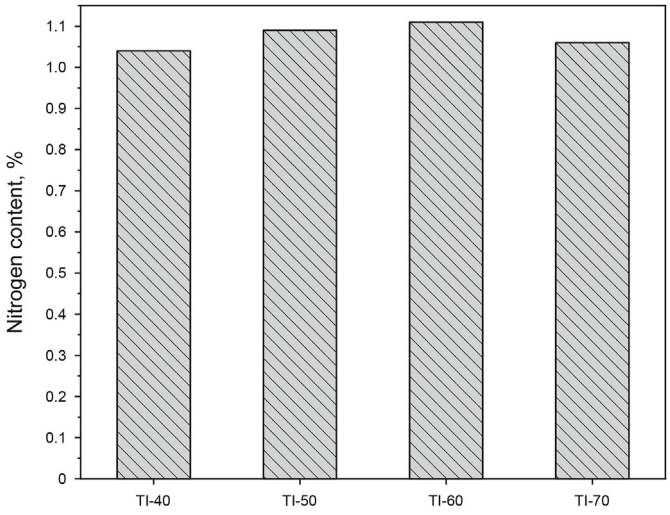

Fig. 15. Nitrogen content of TI-40, TI-50, TI-60, and TI-70.

species of N1 class of Asp-40 with the molecular formula of $C_{50}H_{31}N_1$ (DBE = 36) could be taken as the representative structure of coke. The nitrogen content of TI of 40, 50, 60 and 70 min reactions (short for TI-40, TI-50, TI-60, and TI-70 respectively) were all more than 1% as shown in Fig. 15, and for example, the nitrogen content of typical N1 structures with the molecular formula of $C_{50}H_{31}N_1$ is only about 2%. The coke could contain much N-containing structures with high DBE values like N1 strucuture with the molecular formula of $C_{50}H_{31}N_1$ derived from asphaltenes.

The results obtained clearly indicated that the N-containing asphaltenes with high DBE were sensitive to formation of coke, and at the end of coking induction period N1 class species with the molecular formula of $C_{50}H_{31}N_1$ could be taken as the representative structure of coke. During coking induction period, 1 and 2 ring free radicals without lateral chains would be formed (Dyker et al., 2000; Speybroeck et al., 2003; Ogbuneke et al., 2009), and could be the contributor of formation of N1 structures with the molecular formula of $C_{50}H_{31}N_1$ in termination reaction. As Scheme 2 illustrated, a combination of arylation and cyclization mechanisms of radical reaction pathway was offered as a possible process for the formation of $C_{50}H_{31}N_1$ molecule (Dyker et al., 2000; Speybroeck et al., 2003; Ogbuneke et al., 2009).

The deduced mechanism involving the formation of N1 class species with the molecular formula of $C_{50}H_{31}N_1$ could help give a specific understanding and awareness for coke formation in thermal cracking reaction.

4. Conclusions

For those tested thermal cracking tests, it was observed a coking induction period of 40 min, and the induction period could be greatly prolonged in SHC process. During coking induction period, compared to S1 class species, S2 and S3 and S4 class species of asphaltenes were easily-removed sulfur compounds. While, after coking induction period, the relative abundance of S2 and S3 and S4 classes showed a bit of fluctuations. The faster dealkylation speed could be a key reason, and N-containing (N1, N1S1, N1O1 and N1S1O1) classes' significant decrease could be another reason for the increase of relative abundance of S-containing structures from the end of coking induction period. The remarkable increase in abundance of N1 class before coking induction period could be the reason for the increase of nitrogen content. While at the end and after coking induction period, the asphaltenes formed more coke (TI), which would involve the decrease of N1 class and the reduction of nitrogen content for condensation reaction. Higher polarity N-containing asphaltenes structures have a larger tendency to coke formation. In terms of radical mechanisms reaction pathways, deduced coke formation process was schemed, and N1 structures with 36≤DBE≤40 could be taken as the coke intermediates which could be changed to more condensed aromatic structures of coke or could directly deposit from the liquids as true coke for the phase-separation.

Coke formation process has a unique S and N-containing structures' transfer process. Studying this process not only can help learn more about the coke formation process at molecular level, but also can give a guidance for the heteroatoms removal.

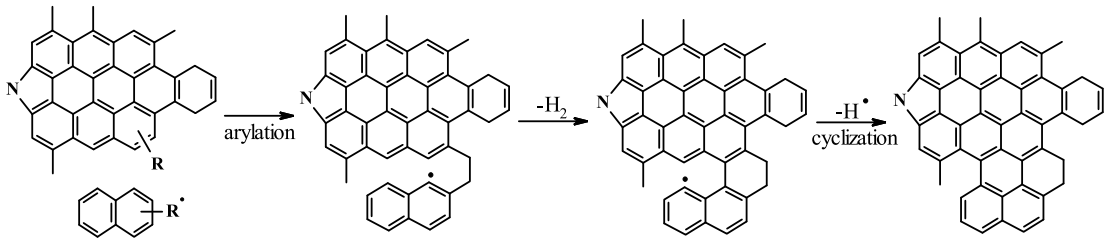

Scheme 2. Coke formation pathway based on condensation of asphaltenes.

Declaration of competing interest

The authors declare that they have no known competing financial interests or personal relationships that could have appeared to influence the work reported in this paper.

Appendix A. Supplementary data

Supplementary data to this article can be found online at https://doi.org/10.1016/j.petsci.2024.01.023.

References

Buenrostro-Gonzalez, E., Groenzin, H., Lira-Galeana, C., et al., 2001. The overriding chemical principles that define asphaltenes. Energy Fuels 15, 972–978. https://doi.org/10.1021/ef0100449.

Chacon-Patino, M.L., Blanco-Tirado, C., Orrego-Ruiz, J.A., et al., 2015. Tracing the compositional changes of asphaltenes after hydroconversion and thermal cracking processes by high-resolution mass spectrometry. Energy Fuels 29, 6330–6341. https://doi.org/10.1021/acs.energyfuels.5b01510.

Chacón-Patiño, M.L., Smith, D.F., Hendrickson, C.L., et al., 2020. Advances in asphaltene petroleomics. Part 4. Compositional trends of solubility subfractions reveal that polyfunctional oxygen-containing compounds drive asphaltene chemistry. Energy Fuels 34, 3013–3030. https://doi.org/10.1021/acs.energyfuels.9b04288.

Chesnokov, V.V., Dik, P.P., Nikityonok, A.V., et al., 2022. Parmon, Comparative analysis of the effects of hydrogen and formic acid on the vacuum residue hydrocracking. Chem. Eng. J. 449, 137839. https://doi.org/10.1016/j.cej.2022.137839.

Cosultchi, A., Garciafigueroa, E., Mar, B., et al., 2002. Contribution of organic and mineral compounds to the formation of solid deposits inside petroleum wells. Fuel 81, 413–421. https://doi.org/10.1016/S0016-2361(01)00187-9.

Dechaine, G., Gray, M., 2010. Chemistry and association of vanadium compounds in heavy oil and bitumen, and implications for their selective removal. Energy Fuels 24, 2795–2808. https://doi.org/10.1021/ef100173j.

Du, H., Liu, D., Li, M., et al., 2015. Effects of the temperature and initial hydrogen pressure on the isomerization reaction in heavy oil slurry-phase hydrocracking. Energy Fuels 29, 626–633. https://doi.org/10.1021/ef5024143.

Dyker, G., Borowski, S., Heiermann, J., et al., 2000. First intermolecular palladium catalyzed arylation of an unfunctionalized aromatic hydrocarbon. J. Organomet. Chem. 606, 108–111. https://doi.org/10.1016/S0022-328X(00)00224-2.

Forero-Franco, R., Cañete-Vela, I., Berdugo-Vilches, T., et al., 2023. Correlations between product distribution and feedstock composition in thermal cracking processes for mixed plastic waste. Fuel 341, 127660. https://doi.org/10.1016/j.fuel.2023.127660.

Gkillas, K., Manickavasagam, J., Visalakshm, S., 2022. Effects of fundamentals, geopolitical risk and expectations factors on crude oil prices. Resour. Pol. 78, 102887. https://doi.org/10.1016/j.resourpol.2022.102887.

Gonçalves, M.L.A., Ribeiro, D.A., Teixeira, A.M.R.F., et al., 2007. Influence of asphaltenes on coke formation during the thermal cracking of different Brazilian distillation residues. Fuel 86, 619–623. https://doi.org/10.1016/j.fuel.2006.08.022.

Gray, M., Tykwinski, R., Stryker, J., et al., 2011. Supramolecular assembly model for aggregation of petroleum asphaltenes. Energy Fuels 25, 3125–3134.

Guo, A., Zhang, X., Wang, Z., 2008. Simulated delayed coking characteristics of petroleum residues and fractions by thermogravimetry. Fuel Process. Technol. 89 (7), 643–650. https://doi.org/10.1016/j.fuproc.2007.12.006.

Hortal, A.R., Hurtado, P., Martínez-Haya, B., et al., 2007. Molecular-weight distributions of coal and petroleum asphaltenes from laser desorption/ionization experiments. Energy Fuels 21, 2863–2868. https://doi.org/10.1021/ef700225s.

Jung, H., Al-Mutairi, A., Hong, I., et al., 2022. Characteristics on catalytic removal of sulfur and nitrogen from atmospheric residues at the molecular level. Catal. Today 388–389, 259–268. https://doi.org/10.1016/j.cattod.2020.06.040.

Kaminski, T., Husein, M.M., 2019. Kinetic modelling of thermal cracking of Arabian atmospheric and vacuum residue. Fuel Process. Technol. 189, 89–97. https://doi.org/10.1016/j.fuproc.2019.03.007.

Li, J., Hou, H., Shen, H., 2022. A new insight into compatibility changing rules for inferior vacuum residue's thermal cracking and hydrocracking process. J. Anal. Appl. Pyrol. 167, 105632. https://doi.org/10.1016/j.jaap.2022.105632.

Li, J.G., She, Y.C., Shen, H.P., et al., 2022. A molecular insight into deoiled asphalt's slurry-phase hydrocracking process. Arab. J. Chem. 15, 104237. https://doi.org/10.1016/j.arabjc.2022.104237.

Mandal, P.C., Wahyudiono, Sasaki, M., et al., 2012. Nickel removal from nickel etioporphyrin (Ni-EP) using supercritical water in the absence of catalyst. Fuel Process. Technol. 104, 67–72. https://doi.org/10.1016/j.fuproc.2011.07.004.

Marques, J., Maget, S., Verstraete, J.J., 2011. Improvement of ebullated-bed effluent stability at high conversion operation. Energy Fuels 25 (9), 3867–3874. https://doi.org/10.1021/ef2006047.

Mullins, O.C., 2010. The modified Yen model. Energy Fuels 24, 2179–2207. https://doi.org/10.1021/ef900975e.

Niles, S.F., Chacón-Patiño, M.L., Smith, D.F., et al., 2020. Comprehensive compositional and structural comparison of coal and petroleum asphaltenes based on extrography fractionation coupled with fourier transform ion cyclotron resonance MS and MS/MS analysis. Energy Fuels 34, 1492–1505. https://doi.org/10.1021/acs.energyfuels.9b03527.

Ogbuneke, K.U., Snape, C.E., Andrésen, J.M., et al., 2009. Identification of a polycyclic aromatic hydrocarbon indicator for the onset of coke formation during visbreaking of a vacuum residue. Energy Fuels 23, 2157–2163. https://doi.org/10.1021/ef801047f.

Pomerantz, A.E., Wu, Q., Mullins, O.C., et al., 2015. Laser-based mass spectroscopic assessment of asphaltene molecular weight, molecular architecture, and nanoaggregate number. Energy Fuels 29, 2833–2842. https://doi.org/10.1021/ef5020764.

Prajapati, R., Kohli, K., Maity, S.K., 2021. Slurry phase hydrocracking of heavy oil and residue to produce lighter fuels: an experimental review. Fuel 288, 119686. https://doi.org/10.1016/j.fuel.2020.119686.

Rana, M.S., Sámano, V., Ancheyta, J., et al., 2007. A review of recent advances on process technologies for upgrading of heavy oils and residua. Fuel 86, 1216–1231. https://doi.org/10.1016/j.fuel.2006.08.004.

Rogel, E., Witt, M., 2017. Asphaltene characterization during hydroprocessing by ultrahigh-Resolution fourier transform ion cyclotron resonance mass spectrometry. Energy Fuels 31, 3409–3416. https://doi.org/10.1021/acs.energyfuels.6b02363.

Sahu, R., Song, B.J., Im, J.S., et al., 2015. A review of recent advances in catalytic hydrocracking of heavy residues. J. Ind. Eng. Chem. 27, 12–24. https://doi.org/10.1016/j.jiec.2015.01.011.

Smyshlyaeva, K.I., Rudko, V.A., Kuzmin, K.A., et al., 2022. Asphaltene genesis influence on the low-sulfur residual marine fuel sedimentation stability. Fuel 328, 125291. https://doi.org/10.1016/j.fuel.2022.125291.

Speybroeck, V.V., Hemelsoet, K., Waroquier, M., et al., 2003. Reactivity and aromaticity of polyaromatics in radical cyclization reactions. Int. J. Quant. Chem. 96, 568–576. https://doi.org/10.1002/qua.10758.

Wang, F., Liu, H., Yu, Y.Y., et al., 2021. Study on the formation of olefinic-bond-containing asphaltenes during thermal cracking of vacuum residue. Fuel 304, 121365. https://doi.org/10.1016/j.fuel.2021.121365.

Wang, L.T., Hu, Y.Y., Wang, L.H., et al., 2021. Visbreaking of heavy oil with high metal and asphaltene content. J. Anal. Appl. Pyrol. 159, 105336. https://doi.org/10.1016/j.jaap.2021.105336.

Wang, T., Liu, Q.Y., Shi, L., et al., 2020. Radicals and coking behaviors during thermal cracking of two vacuum resids and their SARA fractions. Fuel 279, 118374. https://doi.org/10.1016/j.fuel.2020.118374.

Wang, Y., Ren, S., Zhang, L., et al., 2018. Numerical study of air assisted cyclic steam stimulation process for heavy oil reservoirs: Recovery performance and energy efficiency analysis. Fuel 211, 471–483. https://doi.org/10.1016/j.fuel.2017.09.079.

Wattana, P., Fogler, H.S., Yen, A., et al., 2005. Characterization of polarity-based asphaltene subfractions. Energy Fuels 19, 101–110. https://doi.org/10.1021/ef0499372.

Wiehe, I.A., 1993. A phase-separation kinetic model for coke formation. Ind. Eng. Chem. Res. 32 (11), 2447–2454. https://doi.org/10.1021/ie00023a001.

Wiehe, I.A., Liang, K.S., 1996. Asphaltenes, resins and other petroleum macromolecules. Fluid Phase Equil. 117 (1–2), 201–210. https://doi.org/10.1016/0378-3812(95)02954-0.

Xu, Y.M., 2018. Asphaltene Precipitation in paraffinic froth treatment: effects of solvent and temperature. Energy Fuels 32, 2801–2810. https://doi.org/10.1021/acs.energyfuels.7b03013.

Yang, T., Deng, W., Zhu, Y., et al., 2022. The influences of compositional and structural evolutions of asphaltenes on coking behavior during slurry-bed hydrocracking. Fuel 325, 124839. https://doi.org/10.1016/j.fuel.2022.124839.

Yasar, M., Cerci, F.E., Gulensoy, H., 2000. Effect of asphaltenes on pyrolysis kinetics of saturates. J. Anal. Appl. Pyrolysis 56 (2), 219–228. https://doi.org/10.1016/S0165-2370(00)00094-2.

Yasar, M., Trauth, D.M., Klein, M.T., et al., 2001. Asphaltene and resid pyrolysis. 2. The effect of reaction environment on pathways and selectivities. Energy Fuels 15, 504–509. https://doi.org/10.1021/ef0000577.

Zhang, C., Zhang, Y., Liu, M., et al., 2020. Transformation of sulfur compounds in two typical atmospheric residues in hydrotreating via ESI FT-ICR MS. Fuel 281, 118731. https://doi.org/10.1016/j.fuel.2020.118731.

Zhao, J., Liu, T., Han, W., et al., 2021. An insight into the molecular structure of sulfur compounds and their reactivity during residual oil hydroprocessing. Fuel 283, 119334. https://doi.org/10.1016/j.fuel.2020.119334.

Zhao, X., Liu, Y., Xu, C.M., et al., 2013. Separation and characterization of vanadyl porphyrins in Venezuela Orinoco heavy crude oil. Energy Fuels 27, 2874–2882. https://doi.org/10.1021/ef400161p.

Zhong, H., Wei, Z., Man, Y., et al., 2023. Prediction of instantaneous yield of bio-oil in fluidized biomass pyrolysis using long short-term memory network based on computational fluid dynamics data. J. Clean. Prod. 391, 136192. https://doi.org/10.1016/j.jclepro.2023.136192.